Interpretation of the Structure of LEED Intensity Spectra in τ-Matrix Approximation for the Platinum (100) Surface

K. Heinz, N. Lieske, and K. Müller

Institut für Angewandte Physik, Lehrstuhl für Festkörperphysik, Universität Erlangen-Nürnberg

(Z. Naturforsch. **31 a**, 1520–1525 [1976]; received November 13, 1976)

LEED intensity spectra of the clean (00 and $\frac{1}{2}$ 0 beams) and cesium covered ($\frac{1}{2}$ 0 beam) Pt(100) surface at normal or nearly normal incidence are compared with a double diffraction approach developed for the scattering process. A second order scattering approach is always restricted to cases where strong attenuation or weak scattering of the propagating electrons can be assumed. The comparison shows that many (but not all) intensity features of Pt(100) can be attributed to first and second order scattering processes only. Some of the maxima are likely to represent resonances. For proper assignment an effective inner potential is chosen that accounts for slowly varying dynamical effects as well as distortions of the crystal. The approach reveals only interpretations rather than predictions. However, it needs nearly no computational effort.

1. Introduction

LEED intensity spectra generally show a very complicated structure due to the pronounced dynamical character of the diffraction process. The correct theoretical treatment requires a self-consistent multiple scattering theory involving a considerable consumption of computer storage and computing time. This effort, however, can be substantially reduced if the contribution of multiple scattering processes decreases rapidly with the order of these processes e. g. in cases of strong attenuation or weak scattering. Following an approach proposed by Kambe [1] and McRae [2] the total diffraction amplitude can be developed in terms of multiple scattering events at layers. This τ-matrix procedure, which involves the exact diffraction matrix τ for a layer, has been shown successful in second order approximation, even with respect to absolute intensities for materials such as aluminum and copper [3–5]. Moreover, the dynamic calculation of τ can be avoided if the attention is focused on the structure of the intensity spectra only. First and higher order Bragg maxima are predicted from simple Darwin expressions.

This procedure, however, is limited to cases where relevant diffraction orders are known to be low and Bragg conditions are well separated from each other.

The Pt(100) surface is likely to represent another example, to which the second order approximation is applicable. It consists of a hexagonal surface layer followed by quadratic bulk layers [6], a situation very similar to gold [7, 8]. All spots observed in the diffraction pattern can be explained as originating from single and double diffraction processes only at and between the surface layer and bulk layers [8, 9]. Momentum exchange parallel to the surface is dominated by small reciprocal vectors [9]. This limitation as well as the restriction to normal or nearly normal incidence of the primary beam result in a substantial reduction of the number of possible secondary maxima. The paper demonstrates by comparison to what extent LEED intensity maxima of Pt(100) can be attributed to diffraction processes by a second order approach.

Reprint requests to Prof. Dr. K. Müller, Institut für Angewandte Physik, Universität Erlangen-Nürnberg, Erwin-Rommel-Str. 1, *D-8520 Erlangen*.

2. Experiment

The intensity measurements were performed with a combination of a television camera and processing computer. The camera takes the LEED pattern from the luminescent screen and gives its video signal to the computer, which selects one desired diffraction spot by external order. It integrates over the spot area, subtracts simultaneously the background signal and follows the spot with varying energy. Each intensity-energy-point is stored and finally, the division by the separately measured incident current gives the normalized intensity spectrum. For more details of the method see [10]. Each intensity spectrum was taken in less than 8 minutes, this value corresponding to an energy range from 15 to 515 eV and an energy step width of 0.5 eV. The spectra were reproducable with a background pressure of less than $1 \cdot 10^{-9}$ torr. The clean platinum crystal was flashed before running a spectrum. Clean and cesium covered surfaces have been in-

vestigated. The pattern of the latter, which will be discussed elsewhere [9], remained stable for hours. Though spectra of many beams were taken and evaluated, only a few are presented, enough to demonstrate how the second order approximation matches the measurements. These were restricted to normal or nearly normal incidence as it was done in cases of aluminum [3, 4] or silver [11] for reasons mentioned above. The measured intensities of the clean surface agree with other measurements [12] but show more structural details due to background subtraction.

3. Double Diffraction Approach

The τ-matrix approach can be performed by a mathematical development of the full dynamical theory [2] but also, as it is done in this paper, by kinematic summation of layer diffracted amplitudes. In the case of platinum, surface layer and volume layer diffraction must be distinguished because of the surface layer's hexagonal structure [6]. Figure 1 shows the diffraction pattern of the (100) surface (a) which is schematically repeated in (b) where volume layer spots, surface layer spots and mixed spots are distinguished by different symbols. The corresponding diffraction processes can be taken from a schematic diffraction-process-matrix (c). The rows of the matrix represent the order of diffraction processes, the lines indicate the kind of layers involved. So the first row corresponds to first order diffraction contributions and the second and third row to second order ones, distinguished by the sequence of forward and backward scattering. With each additional diffraction order n additional 2^{n-1} rows would occur, giving a total of 2^n-1 processes.

To gain an expression for one double diffraction contribution the diffraction behaviour of the layers is needed. Let $\varrho(\boldsymbol{K}, \boldsymbol{K}')$ be the diffraction amplitude for a volume layer describing the elastic transition of a wave $\exp(i\boldsymbol{K}\cdot\boldsymbol{r})$ impinging onto the plane to the one $\exp(i\boldsymbol{K}'\cdot\boldsymbol{r})$ leaving the plane. Then $\tau(\boldsymbol{K}) = 1+\varrho(\boldsymbol{K}, \boldsymbol{K})$ stands for the transmission amplitude. $\boldsymbol{R}$ denotes the displacement vector between neighboured volume layers and $\hat{\varrho}$, $\hat{\tau}$, $\hat{\boldsymbol{R}}$ indicate the respective values for the surface layer. Then, for example, the secondary contribution M_{12} in the scattering-process-matrix in Fig. 1 c can be calculated by adding the corresponding infinite number of amplitudes [5]. Attenuation ($\mathrm{Im}\,K>0$ and/or $|\tau|<1$) makes the sum converge to

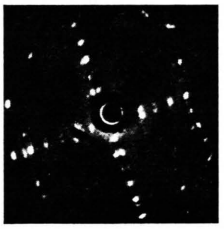

(a)

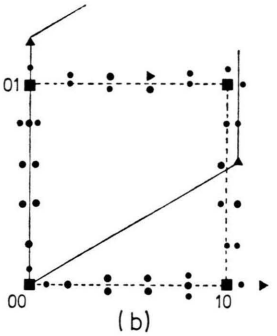

(b)

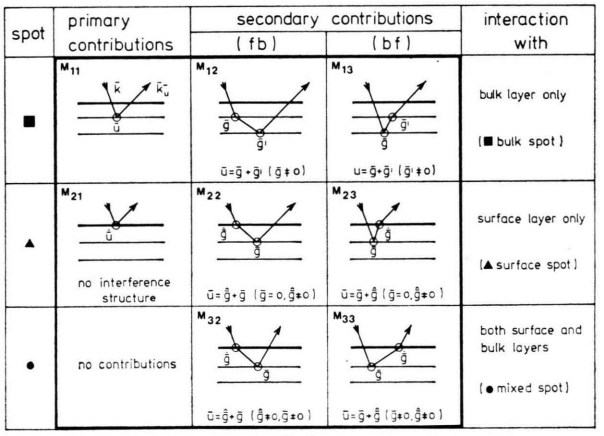

(c)

Fig. 1. (a) LEED pattern of the clean Pt(100) surface at $E=60$ eV. (b) Schematic LEED pattern with surface layer spots ▲ (hexagonal unit mesh ———), bulk layer spots ■ (quadratic unit mesh — — —) and mixed spots ●, arising at various energies. (c) Diffraction process matrix (fb = first forward and then backward scattering, bf vice verca). Interaction means that momentum parallel to the layer is exchanged.

$$A_{12}=\sum_{\boldsymbol{g}\neq 0}\frac{\hat{\tau}(\boldsymbol{K})\,e^{i\boldsymbol{K}\cdot\hat{\boldsymbol{R}}}\,\varrho(\boldsymbol{K},\boldsymbol{K}_{\boldsymbol{g}}^{+})\,\varrho(\boldsymbol{K}_{\boldsymbol{g}}^{+},\boldsymbol{K}_{\boldsymbol{u}}^{-})\,e^{i\boldsymbol{K}_{\boldsymbol{u}}^{-}\cdot\hat{\boldsymbol{R}}}\,\hat{\tau}(\boldsymbol{K}_{\boldsymbol{u}}^{-})\,\tau(\boldsymbol{K}_{\boldsymbol{u}}^{-})\,e^{i\boldsymbol{K}_{\boldsymbol{g}}^{+}\cdot\boldsymbol{R}}\,e^{i\boldsymbol{K}_{\boldsymbol{u}}^{-})\cdot\boldsymbol{R}}}{\{1-\tau(\boldsymbol{K})\cdot\tau(\boldsymbol{K}_{\boldsymbol{u}}^{-})\,e^{i(\boldsymbol{K}-\boldsymbol{K}_{\boldsymbol{u}}^{-})\cdot\boldsymbol{R}}\}\cdot\{1-\tau(\boldsymbol{K}_{\boldsymbol{g}}^{+})\,\tau(\boldsymbol{K}_{\boldsymbol{u}}^{-})\,e^{i(\boldsymbol{K}_{\boldsymbol{g}}^{+}-\boldsymbol{K}_{\boldsymbol{u}}^{-}\cdot\boldsymbol{R}}\}}\,. \tag{1}$$

Here $\boldsymbol{K}_{\boldsymbol{g}}^{\pm}(\boldsymbol{K}_{\boldsymbol{u}}^{\pm})$ is the wave vector which results when the undisturbed wave with vector $\boldsymbol{K}$ exchanges the vector $\boldsymbol{g}(\boldsymbol{u})$ with the crystal. The + and − signs indicate the propagating direction, i. e. into and out of the crystal, respectively. The vector $\boldsymbol{u}$ is the totally exchanged vector whilst $\boldsymbol{g}$ is that vector exchanged in the first diffraction process. For the other contributions M_{ik} similar expressions are derived as well. Primary contributions show only one Darwin factor of the form

$$[1-\tau(\boldsymbol{K})\tau(\boldsymbol{K}_{\boldsymbol{u}}^{-})\exp\{i(\boldsymbol{K}-\boldsymbol{K}_{\boldsymbol{u}}^{-})\cdot\boldsymbol{R}\}]$$

as denominator.

It has been shown for other materials such as aluminum and copper that the double diffraction approach already shows the main features of the intensity spectra when $\varrho(\boldsymbol{K},\boldsymbol{K}')$ is calculated exactly [3, 5, 13]. Unfortunately selfconsistent numerical efforts are again involved. However these efforts could be avoided if $\varrho(\boldsymbol{K},\boldsymbol{K}')$ varies only smoothly with energy. Then the maxima (structure) of the diffraction amplitude are given by the minima of the amplitude denominator, which again are given by the oscillatory behaviour of the denominator exponentials (Bragg energies).

The justification for this kinematic evaluation of double diffraction contributions must be tested by investigation of $\varrho(\boldsymbol{K},\boldsymbol{K}')$, which has been performed for Cu, Fe and W layers [14]. The general feature is that ϱ makes up a smooth function of energy, except a few maxima. This is believed to be true for layers consisting of only one plane of atoms. The exceptional maxima correspond to resonant states with pronounced intralayer scattering. In most cases we found resonant and Bragg energies well enough separated for identification. It should be pointed out, however, that the attribution of intensity structure to certain scattering processes will fail when maxima of different origin coincide and interfere.

4. Peakenergies

(a) Bragg Peaks

The smooth single layer scattering behaviour (apart from resonant regions) makes the primary Bragg peaks appear at their kinematic energies, i. e. for real τ if the condition

$$(\boldsymbol{K}-\boldsymbol{K}_{\boldsymbol{u}}^{-})\cdot\boldsymbol{R}=2\pi n, n=1,2,3\ldots \qquad (2)$$

is fullfilled. Here again $\boldsymbol{u}$ denotes the spot under consideration and n stands for the order of the peak. For complex values of τ, (2) must be modified. We will return to this point in Section 5.

The secondary Bragg peak energies can be derived from (1) in a similar way. As the denominator factorizes into two Darwin factors, two maxima arise. Neglecting their mutual influence, one of them is given by (2) and the other by

$$(\boldsymbol{K}_{\boldsymbol{g}}^{+}-\boldsymbol{K}_{\boldsymbol{u}}^{-})\cdot\boldsymbol{R}=2\pi n, n=1,2,3,\ldots . \qquad (3)$$

Similarly, for the process M_{13} in Fig. 1 c, the maximum condition is given by

$$(\boldsymbol{K}-\boldsymbol{K}_{\boldsymbol{g}}^{-})\cdot\boldsymbol{R}=2\pi n, n=1,2,3,\ldots , \qquad (4)$$

and all other conditions derive in the same way.

(b) Resonance Peaks

Maxima of the total diffraction amplitude can also occur by maxima of the diffraction behaviour of the layer. This is due to the excitation of an electronic eigenstate (resonance) of the layer [14], i. e. the diffracted wave runs within the layer itself. Therefore the resonant energy is given by

$$(\boldsymbol{K}_{\boldsymbol{g}})_{\perp}=0 . \qquad (5)$$

It seems to be sufficient to expect resonance contributions only from the surface layer. Succeeding layers are less likely to be excited because of attenuation.

5. Inner Potential

The numerical energy values satisfying conditions (2 – 5) are also influenced by the (unknown) inner potential, which makes the electron wave vector increase when entering the crystal. It can be derived from the spectra if first order Bragg peaks can be clearly identified, i. e. if pronounced and Lorentzian shaped peaks occur. This is possible in many cases (e. g. nickel [15]) and most probable at normal incidence [11]. It is also true for platinum, as can be seen in Fig. 2 a, where clear peaks occur for $n=3,\ldots,7$ in the specular spot spectrum. The evaluation of (2) using the bulk value of $\boldsymbol{R}$ gives an energy dependent inner potential shown in Figure 2 b. It is used to correct all other positions of secondary peaks and resonances.

The muffin tin model of the solid interpretes the inner potential as the spatial constant potential V_0 between ion cores, which usually shows no strong

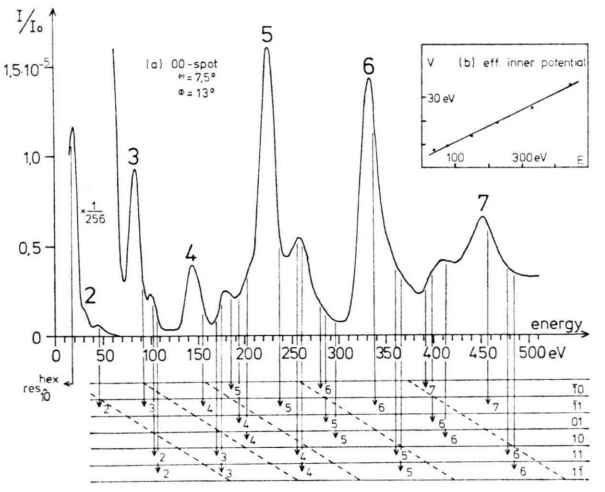

Fig. 2. (a) Intensity-energy spectrum of the 00-spot of the platinum (100) surface for nearly normal incidence ($\Theta = 7.5°$, $\Phi = 13°$). Below: Identification of the maxima. The lines indicate the reciprocal vectors exchanged parallel to the surface, the diagonal rows give the order of interference. (b) Effective inner potential derived from the primary Bragg peaks of (a).

energy dependence as it was explicitely shown for nickel [16]. Thus the evaluated energy dependence in Fig. 2 b must be caused by deviations from the idealizing assumptions we made for the calculation of intensity peaks. Therefore we will use the name "effective inner potential" in the following.

First of all the neglected energy dependence of the layer diffraction amplitude ϱ might be responsible for the observed behaviour of V_{eff}. Moreover the peak positions were evaluated assuming real transmission amplitudes τ. In general this is not true and so condition (2), for example, modifies to $(\boldsymbol{K} - \boldsymbol{K}_{\boldsymbol{u}}^{-}) \cdot \boldsymbol{R} = (2\pi n - 2\varphi)$ where φ is the phase of τ. This again leads to a contribution to the effective inner potential if φ is neglected. A quantitative calculation for a nickel crystal gives a linearly increasing contribution, which saturates at $2-3$ eV above $E = 200$ eV [17]. In this way part of dynamical effects, which normally shift peak positions, are considered by the correction with the effective inner potential.

Another possible contribution to V_{eff} may arise from a step like behaviour of V_0 at the surface or from a possible deviation of the first layer distance from the bulk value. In the latter case the incident electron transverses a mean distance which depends on the penetration depth. In the simplest case only the top layer distance, a, differs from the bulk value, b. Then for low temperatures, a simple calculation gives the new Bragg maxima positions for the specular beam at $E = E_0 - \{E_0\,\delta(1-p^2)^2 + V_0\}$. Here E_0 is the position of the undisturbed maximum, $\delta = (a-b)/b \ll 1$ denotes the surface expansion and p the attenuation factor for propagation from one layer to the next. The term in parenthesis could be identified as a contribution to the effective inner potential. However at room temperatures the relative contribution of coherent scattering of the surface layer becomes smaller compared with bulk layers because of the increased vibrational amplitude of surface atoms. For platinum with a Debye temperature of $\Theta \approx 230$ K this is essentially true for $E > 300$ eV. Then a more complicated expression for the energy shift results. Of course it's influence can be still considered by an energy dependent effective inner potential.

6. Intensity Spectra Interpretation

With the inner potential corrections, which are evaluated for each beam separately, the conditions $(3-5)$ immediately give the numerical values for secondary Bragg energies and resonances. Evaluating expressions (3) and (4) for volume layer spots gives with $\boldsymbol{K} = (\boldsymbol{K}_{\|}, K_{\perp})$ and $\boldsymbol{R} = (\boldsymbol{R}_{\|}, b)$

$$\sqrt{K^2 - (\boldsymbol{K}_{\|} + 2\pi\boldsymbol{g})^2} + \sqrt{K^2 - (\boldsymbol{K}_{\|} + 2\pi\boldsymbol{u})^2} = (2\pi/b)\,[n + (\boldsymbol{u} - \boldsymbol{g}) \cdot \boldsymbol{R}_{\|}] \quad (3')$$

for process M_{12}

and

$$K_{\perp} + \sqrt{K^2 - (\boldsymbol{K}_{\|} + 2\pi\boldsymbol{g})^2} = (2\pi/b)\,(n + \boldsymbol{g} \cdot \boldsymbol{R}_{\|}) \quad (4')$$

for process M_{13}

respectively, where $\boldsymbol{g}$ and $\boldsymbol{u}$ are the intermediately and totally exchanged reciprocal lattice vectors. For surface layer spots the process M_{21} in Fig. 1 c can show no interference structure. The structure of process M_{22} is deduced from (3′) with $\boldsymbol{g} = 0$, $\boldsymbol{u} = \hat{\boldsymbol{g}}$ and that of M_{23} results from (4′) simply with $\boldsymbol{g} = 0$. The conditions for the mixed spots M_{32} and M_{33} in Fig. 1 c follow similarly.

For (fcc) crystals, $\boldsymbol{g} \cdot \boldsymbol{R}_{\|} = (m/2)$ with m integer. Therefore, condition (3′) and (4′) coincide for the specular beam ($\boldsymbol{u} = 00$, $\boldsymbol{g} = -\boldsymbol{g}'$), leading to a very simple interpretation of the 00-spectrum. At normal incidence, symmetric processes like $00 = 10 + \bar{1}0$ and $00 = 01 + 0\bar{1}$ would degenerate but the incidence angle $\Theta = 7.5°$ brakes the degeneracy. The calculated values are shown in the table below

the spectrum in Fig. 2 a, where the lines indicate the momentum exchanged and the diagonal subdivision gives the order of interference. It can be seen that possible peak energies coincide with the really observed structure. In most cases the nearly normal incidence only broadens the peaks which can still be properly associated with nearly equivalent diffraction processes.

However, it must be underlined, that, since absolute intensities were a priori renounced, it cannot be predicted whether a secondary peak really arises or not. But if it arises, we feel it can be identified with respect to the basic scattering process in case of Pt. This is of particular value for the resonance peaks which are most sensible to the surface layer structure and so to adsorption. For platinum resonances only occur by exchange of hexagonal reciprocal vectors. So $\hat{\boldsymbol{g}} = \hat{1}0$ (equivalent with $\boldsymbol{g} = \frac{6}{5}0$) gives with (5) a resonance at about 21 eV which appears with considerable weight and is broadened by broken degeneracy. The fact that this peak disappears rapidly already with beginning adsorption of cesium supports its identification as resonance. This on the other hand is a weighty indication for the also otherwise guessed fact, that the hexagonal surface layer of Pt(100) reorganizes to a square mesh structure during adsorption. Moreover, from this new top layer, the occurence of a new resonance can be expected, corresponding to the exchange of a reciprocal vector of the square mesh. This indeed is observed in the intensity of the specular beam, which is not shown here because of shortness.

The demonstrated structure analysis is successful for the other spots, too. In most cases where secondaries do not appear as peaks they are hidden in the broadening of other peaks, secondaries and primaries as well. Most interesting, however, should be the mixed spots, which in the model adopted here occur by double diffraction only. They cannot show the usual primary Bragg peak structure, which requires that each layer can exchange a "mixed" reciprocal vector. This might be true with some weight for the surface layer because of spuckling [12, 17] but is more unlikely for the following layers. Moreover, contributions arising from such a distortion of the surface layer are expected to be considerable only for energies above 50 eV [18]. In this range, however, the measured intensities become considerable weak (Figure 3 a). So the structure of mixed spots is mainly given by the structure of the beams from which they result by double diffraction. Therefore tertiary contributions may become important particularly in the intensities of mixed spots. This is shown in Fig. 3 a for the $\frac{1}{5}$ 0-spot of the clean surface for nearly normal incidence which consists of a diffraction event $\hat{1}0$ at the surface layer followed by $\bar{1}0$ at a volume layer or vice versa. When the first diffraction process happens at the surface layer (process M_{31} in Fig. 1 c), the Bragg conditions for the 10-beam must be evaluated for oblique incidence. Similarly for process M_{33} (first $\bar{1}0$ and then $1\hat{0}$) maxima arise due to the Bragg primaries of the $\bar{1}0$ beam for normal incidence (in general the different processes are distinguished by the sequence of forward and backward scattering giving the notations fb or bf). However when looking at the $\bar{1}0$-spectrum (not shown), we see that its primaries are of low intensity in the relevant energy range and are dominated by a heavy secondary Bragg peak at 52 eV. Thus only the latter shows up in the $\frac{1}{5}$ 0-spectrum and is symbolized by $\text{sek}_{\bar{1}0}$. The first maximum in the spectrum is believed to represent the $\hat{1}0$ resonance.

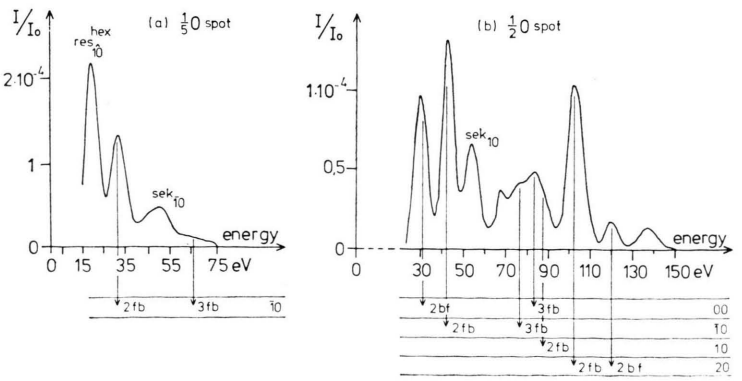

Fig. 3. (a) Spectrum and interpretation of the $\frac{1}{5}$ 0-spot of the clean platinum (100) surface for nearly normal incidence ($\Theta = 2.5°$, $\Phi = 13°$). (b) Spectrum and interpretation of the $\frac{1}{2}$ 0-spot of the cesium covered (2×1) platinum (100) surface for normal incidence.

The adsorption of cesium on the Pt(100) surface causes the complicated superstructure of the clean surface to disappear and gives rise to a (2×1) structure with streaking. The adsorption model for this structure is not quite simple due to the size of the cesium atoms [9]. However, for the interpretation of the measured intensity structures it is sufficient to know, that the surface layer may exchange half order wave vectors with the incident electron beam. Consequently all hexagonal resonance structures disappear in the spectra and are replaced (in some spectra) by new resonances corresponding to the (2×1) surface layer. We restrict our demonstration to the intensity of the $\frac{1}{2}0$-spot which is shown in Figure 3 b. The spot is built up by the construction $\frac{1}{2}0=00+\frac{1}{2}0=\frac{1}{2}0+00=10+\frac{\bar{1}}{2}0=\frac{\bar{1}}{2}0+10=\frac{3}{2}0+\bar{1}0=\bar{1}0+\frac{3}{2}0=20+\frac{\bar{3}}{2}0=\frac{\bar{3}}{2}+20$ from which corresponding peaks are calculated. No peaks arise from the processes $10+\frac{\bar{1}}{2}0$ and $\frac{\bar{1}}{2}0+10$ because of the low 10-intensity in the relevant range. Two peaks remain unidentified, again indicating that higher order processes may be important for the structure of mixed spot spectra.

Conclusion

Finally it should once more be pointed out that the described interpretation in terms of subsequent scattering processes is only reasonable if all three main assumptions and approximations can simultaneously be made:

(a) Higher order diffraction processes make only negligible contributions to the total amplitude with respect to structure. This is approximated in the case of strong attenuation and is likely to be true for Pt(100) supported by a double diffraction model for its superstructure. For medium attenuation or mixed spots which show no primary peaks higher order contributions may occur. Peak identification for normal or nearly normal incidence more than peak prediction is suitable within the procedure.

(b) The single layer diffraction behaviour has to vary slowly with energy compared to the behaviour of Darwin factors except for a few resonance energies. These should be separated from Bragg peaks by at least several volts which is also required for the secondary peaks.

(c) Disturbances of the ideal kinematic parameters as surface layer dilatation, phase shift of a beam by crossing a layer or additional surface potential steps can be taken into account by an energy dependent effective inner potential. Its variation with energy must be slow enough, to make interpolation between primary Bragg peaks possible.

Acknowledgement

This work was supported by Deutsche Forschungsgemeinschaft.

[1] K. Kambe, Z. Naturforsch. **22 a**, 322 [1967]; **23 a**, 1280 [1968].
[2] E. G. McRae, Surface Sci. **11**, 479, 492 [1968].
[3] V. Hoffstein and G. Albinet, Surface Sci. **38**, 506 [1973].
[4] C. B. Duke, G. E. Laramore, B. W. Holland, and A. M. Gibbons, Surface Sci. **27**, 523 [1971].
[5] P. J. Jennings, Surface Sci. **41**, 67 [1974].
[6] A. E. Morgan and G. A. Somorjai, Surface Sci. **12**, 405 [1968].
[7] D. G. Fedak and N. A. Gjostein, Surface Sci. **8**, 77 [1967].
[8] P. W. Palmberg and T. N. Rhodin, J. Chem. Phys. **49**, 134 [1968].
[9] K. Müller, P. Heilmann, K. Heinz, and G. G. Waldecker, Vak. Techn. **8**, 227 [1976].
[10] P. Heilmann, E. Lang, K. Heinz, and K. Müller, Appl. Phys. **9**, 247 [1976].
[11] M. P. Seah, Surface Sci. **17**, 181 [1969].
[12] T. A. Clarke, R. Mason, and M. Tescari, Surface Sci. **40**, 1 [1973].
[13] G. Albinet, R. Baudoing, D. Aberdam, and V. Hoffstein, Surface Sci. **42**, 467 [1974].
[14] K. Kambe, Surface Sci. **20**, 213 [1970].
[15] J. E. Demuth and T. N. Rhodin, Surface Sci. **42**, 261 [1974].
[16] J. B. Pendry, J. Phys. C (Solid St. Phys.), Ser. 2, **2**, 1215 [1969].
[17] J. B. Pendry, J. Phys. C: Solid State Phys. **5**, 2567 [1972].
[18] P. W. Palmberg and T. N. Rhodin, J. Chem. Phys. **49**, 147 [1968].